Inversion of Potential Vorticity Density

JOSEPH EGGER

Meteorological Institute, University of Munich, Munich, Germany

KLAUS-PETER HOINKA

Institute for Atmospheric Physics, Deutsches Zentrum für Luft- und Raumfahrt, Oberpfaffenhofen, Germany

THOMAS SPENGLER

Geophysical Institute, University of Bergen, Bergen, Norway

(Manuscript received 30 April 2016, in final form 7 December 2016)

ABSTRACT

Inversion of potential vorticity density $P_\eta^* = (\boldsymbol{\omega}_a \cdot \nabla\eta)/(\partial\eta/\partial z)$ with absolute vorticity $\boldsymbol{\omega}_a$ and function η is explored in η coordinates. This density is shown to be the component of absolute vorticity associated with the vertical vector of the covariant basis of η coordinates. This implies that inversion of P_η^* in η coordinates is a two-dimensional problem in hydrostatic flow.

Examples of inversions are presented for $\eta = \theta$ (θ is potential temperature) and $\eta = p$ (p is pressure) with satisfactory results for domains covering the North Pole. The role of the boundary conditions is investigated and piecewise inversions are performed as well. The results shed new light on the interpretation of potential vorticity inversions.

1. Introduction

Potential vorticity (PV) is an important variable in dynamic meteorology and oceanography and is widely used for the simulation and interpretation of a broad range of flow phenomena (e.g., Vallis 2006), where potential vorticity is

$$Q_\eta = \frac{\boldsymbol{\omega}_a \cdot \nabla\eta}{\rho}, \tag{1}$$

and $\boldsymbol{\omega}_a$ is absolute vorticity, η is a function of space and time, and ρ is density (Ertel 1942). Use of Q_η is not widespread except for $\eta = \theta$ (θ is potential temperature) where Q_θ is conserved in adiabatic and inviscid flow. The explicit expression for Q_η in spherical coordinates is fairly complicated:

$$\begin{aligned} Q_\eta\rho = &\left(-\frac{\partial v}{\partial z} + a^{-1}\frac{\partial w}{\partial\varphi}\right)(a\cos\varphi)^{-1}\frac{\partial\eta}{\partial\lambda} \\ &+ \left[\frac{\partial u}{\partial z} - (a\cos\varphi)^{-1}\frac{\partial w}{\partial\lambda}\right]a^{-1}\frac{\partial\eta}{\partial\varphi} \\ &+ (a\cos\varphi)^{-1}\left[\frac{\partial v}{\partial\lambda} - \frac{\partial}{\partial\varphi}(u\cos\varphi)\right]\frac{\partial\eta}{\partial z} + f\frac{\partial\eta}{\partial z}, \end{aligned} \tag{2}$$

with standard notation (longitude λ; latitude φ; height z; velocity components u, v, and w; Coriolis parameter $f = 2\Omega\sin\varphi$ with $\Omega = 2\pi\,\text{day}^{-1}$; and Earth's radius a). The traditional approximation is accepted in (2), where we assume $r = a + z \approx a$ and neglect Coriolis terms with $2\Omega\cos\varphi$ (e.g., Vallis 2006). A simplification can be obtained by selecting η as a vertical coordinate and turning to PV density (PVD) $P_\eta = Q_\eta\rho$. We have to realize, however, that P_η is a density in (λ, φ, z) space, but not in (λ, φ, η) space, as would be appropriate in η coordinates. We introduce the density $P_\eta^* = P_\eta(\partial z/\partial\eta)$ to ensure that volume integrals of P_η in height coordinates equal those of P_η^* in η coordinates.

The transformation of (2) to η coordinates can be performed by introducing the covariant basis vectors

Corresponding author e-mail: Joseph Egger, j.egger@lrz.uni-muenchen.de

DOI: 10.1175/JAS-D-16-0133.1

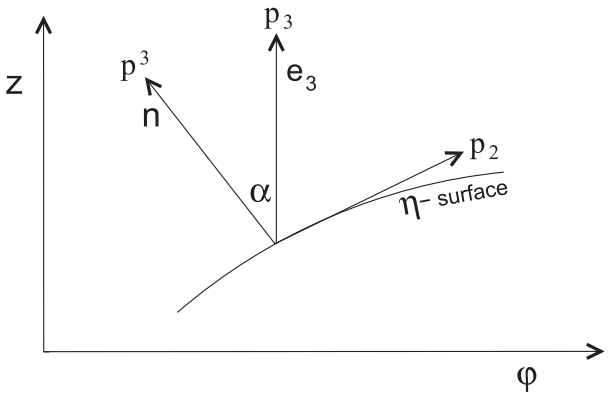

FIG. 1. Orientation of the various basis and vorticity vectors with respect to an η surface.

$$\mathbf{p}_1 = a\cos\varphi\mathbf{e}_1 + \left.\frac{\partial z}{\partial\lambda}\right|_\eta \mathbf{e}_3,$$
$$\mathbf{p}_2 = a\mathbf{e}_2 + \left.\frac{\partial z}{\partial\varphi}\right|_\eta \mathbf{e}_3,$$
$$\mathbf{p}_3 = \frac{\partial z}{\partial\eta}\mathbf{e}_3, \tag{3}$$

where $\mathbf{e}_i$ are the standard spherical unit vectors with $\mathbf{e}_1$ pointing eastward, $\mathbf{e}_2$ pointing northward, and $\mathbf{e}_3$ pointing upward [e.g., Zdunkowski and Bott (2003), see their Fig. 1]. The first two vectors are embedded in η surfaces and orthogonal to $\nabla\eta = \mathbf{p}^3$ with contravariant basis vector $\mathbf{p}^3$, where $\mathbf{p}^3 \cdot \mathbf{p}_i = \delta_i^3$. Next we have to adapt the derivatives in (2) to the η system so that the absolute vorticity, after expressing all $\mathbf{e}_i$ in terms of $\mathbf{p}_i$, becomes

$$\begin{aligned}\boldsymbol{\omega}_a = (a\cos\varphi)^{-1}&\left[-\frac{\partial v}{\partial\eta}\frac{\partial\eta}{\partial z} + a^{-1}\left(\frac{\partial w}{\partial\varphi} - \frac{\partial w}{\partial\eta}\frac{\partial\eta}{\partial z}\frac{\partial z}{\partial\varphi}\right)\right]\mathbf{p}_1\\ &+ a^{-1}\left[\frac{\partial u}{\partial\eta}\frac{\partial\eta}{\partial z} - (a\cos\varphi)^{-1}\left(\frac{\partial w}{\partial\lambda} - \frac{\partial w}{\partial\eta}\frac{\partial\eta}{\partial z}\frac{\partial z}{\partial\lambda}\right)\right]\mathbf{p}_2\\ &+ \left[\zeta_\eta - (a\cos\varphi)^{-1}\left(\frac{\partial z}{\partial\lambda}\frac{\partial w}{\partial\varphi} - \frac{\partial z}{\partial\varphi}\frac{\partial w}{\partial\lambda}\right) + f\right]\frac{\partial\eta}{\partial z}\mathbf{p}_3,\end{aligned} \tag{4}$$

with

$$\zeta_\eta = (a\cos\varphi)^{-1}\left[\frac{\partial v}{\partial\lambda} - \frac{\partial(u\cos\varphi)}{\partial\varphi}\right], \tag{5}$$

where all "horizontal" derivatives are performed for constant η and $z(\lambda, \varphi, \eta)$ is the height of η surfaces. The final step consists in multiplying (4) by $(\partial z/\partial\eta)\mathbf{p}^3$, so that

$$P_\eta^* = \zeta_\eta - (a\cos\varphi)^{-1}\left(\frac{\partial z}{\partial\lambda}\frac{\partial w}{\partial\varphi} - \frac{\partial z}{\partial\varphi}\frac{\partial w}{\partial\lambda}\right) + f. \tag{6}$$

On the other hand, P_η results if we multiply (4) by $\mathbf{p}^3$. An alternative derivation of (6) is provided by Viúdez (2001).

Because $(\partial\eta/\partial z)\mathbf{p}_3 = \mathbf{e}_3$ in (4) is a unit vector and because we may replace $\mathbf{p}_1$ and $\mathbf{p}_2$ in (4) by unit vectors $\mathbf{p}_i/|\mathbf{p}_i|$ multiplied by $|\mathbf{p}_i|$, we see that P_η^* is the vertical component of absolute vorticity with respect to a nonorthogonal basis of unit vectors parallel to the covariant ones. In particular, ζ_η is the related vertical component of relative vorticity in hydrostatic flow where $w = 0$ in (4)–(6). This interpretation differs somewhat from others found in the literature. For example, McIntyre (2015) claims that "the isentropic vorticity... is the same as the component of the vorticity vector normal to the isentropic surface" (p. 376). This definition converges to ours for steepness $\alpha \to 0$ (see Fig. 1). Small values of α are typical of isentropic surfaces in large-scale flow, but the vorticity must be formulated with respect to the nonorthogonal vector basis to be correct also for steep surfaces as found, for example, in PV banners (Schär et al. 2003). In what follows we will concentrate on hydrostatic flows so that $P_\eta^* = \zeta_\eta + f$. This formula is well known for isentropic flow.

With P_η^* available we can now turn to inversion. PV inversion (PVI) is one of the most popular applications of PV thinking (Hoskins et al. 1985), which is used to derive winds, pressure, and temperature from a Q_η field on the basis of a balance condition and suitable boundary conditions (e.g., Thorpe 1985; Hoskins et al. 1985). However, inversion of Q_η is difficult owing to the nonlinearity of Q_η so that iterative methods have to be used (e.g., Davis 1992). This problem can be partly overcome by recognizing that invertibility is not restricted to PV (Egger and Hoinka 2010). In particular, we may perform an inversion of P_η^* (PVDI) in η coordinates. For example, P_θ^* is a linear two-dimensional expression on isentropic surfaces [see (6)], so that inversion is relatively simple.

Although Q_θ is materially conserved for adiabatic and inviscid flow, all other choices of PV like Q_p are not conserved nor are P_η and P_η^*. Thus, Q_θ can be stepped forward with the winds obtained from the inversion, while that is not possible for Q_p and P_η and P_η^*. However, as will be discussed in detail below, inversion of P_θ^* allows to evaluate Q_θ so that the inversions of Q_θ and P_θ^* are equivalent with respect to eventual predictions. Moreover, PVDI is of interest by itself, because it attributes the flow on an η surface to the vorticity ζ_η on that surface, at least for geostrophic balance, as will be shown below. PVI would attribute the flow to the three-dimensional field Q_η. Thus, the same flow can be attributed to different "sources" depending on the variable selected for inversion.

It is the purpose of this short contribution to present inversions of P_θ^* and also of P_p^* based on

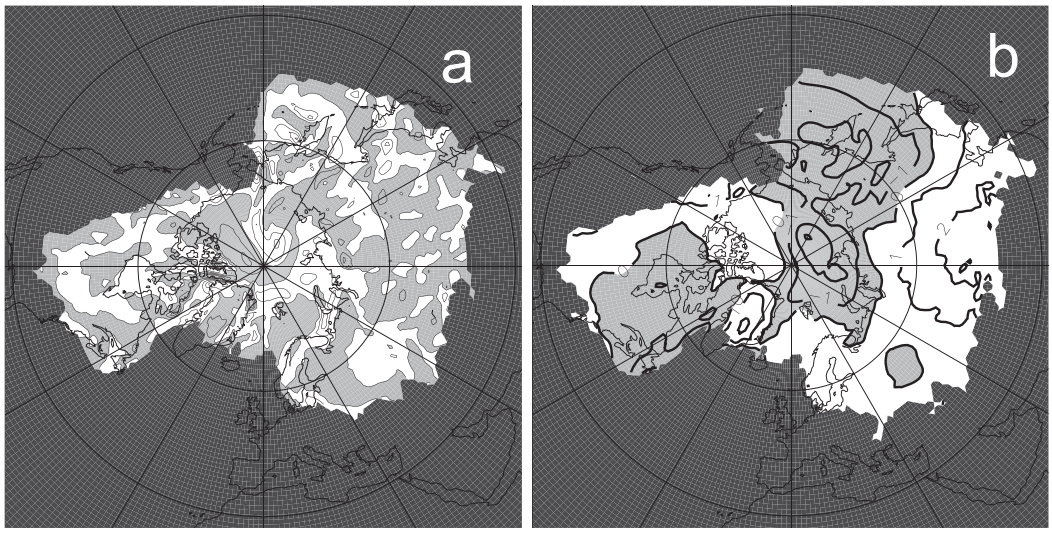

FIG. 2. Vorticity and Montgomery potential on the $\theta = 285$-K surface at 0000 UTC 12 Feb 2008: (a) vorticity ($10^{-4}\,s^{-1}$; contour interval = $0.5 \times 10^{-4}\,s^{-1}$) and (b) Montgomery potential on $\theta = 285$ K ($10^3\,m^2\,s^{-2}$; contour interval = $1.0 \times 10^3\,m^2\,s^{-2}$). Negative values and areas outside the intersection contour are shaded. Mean value $\overline{M} = 0.277 \times 10^6\,m^2\,s^{-2}$ subtracted in (b).

observations to demonstrate the feasibility of this approach and to discuss the interpretation of inversions.

2. Inversion of potential vorticity density

As stated above, PVI is a well explored and widely used technique to approximately capture all dynamic information about a flow state (e.g., Thorpe 1985). Only PV has to be known, if a balance relation is imposed together with appropriate boundary conditions. PVI has mainly been carried out for Q_θ in pressure coordinates.

Piecewise potential vorticity inversion (PPVI) goes one step further by seeking to determine the flow fields associated with isolated PV anomalies. This technique has been used to understand, for example, the impact of observed PV anomalies on hurricane development (Davis and Emanuel 1991) or the influence of upper-level PV features on the evolution of polar lows (Bracegirdle and Gray 2009). We wish to invert P^*_η for $\eta = \theta$ and $\eta = p$, where the main step involves the derivation of the flow on an η surface from observed ζ_η on that surface. Piecewise inversions will be carried out as well.

In general, a streamfunction ψ can be obtained by inverting $\Delta_2\psi = \zeta_\eta$, with two-dimensional Laplacian Δ_2. This is a linear problem. Geostrophic balance, or a more advanced balance condition like that of Charney (1955), must then be used to obtain, for example, the Montgomery potential $M = c_pT + gz$ for $\eta = \theta$ or the geopotential ϕ for $\eta = p$. Although the latter condition is nonlinear with respect to ψ, it is linear with respect to M or ϕ.

a. Inversion of P^*_θ

We select the distribution of P^*_θ on the surface $\theta = 285$ K in the Northern Hemisphere for a demonstration of PVDI (see Fig. 2). The date in Fig. 2 has been chosen randomly, as we do not aim to perform a dynamic analysis of a certain flow configuration. The main purpose of this presentation is to discuss PVDI as a method.

The $\theta = 285$-K surface intersects Earth's surface all around the North Pole on that day and forms a dome north of the intersection contour. The observed vorticity ζ_θ on this surface, as determined from ERA-Interim (Dee et al. 2011), is fairly patchy, but there are several stripes of positive as well as negative vorticity extending from the southern boundary almost to the pole (Fig. 2a). The observed M perturbations are dominated by a huge ridge covering much of western Eurasia and a system of lows closer to the pole (Fig. 2b), where a northward decrease of M implies westerly flow. The scale of the observed M perturbations, defined as the deviation from the areal mean, is much larger than that of ζ_θ, as expected.

Accepting geostrophic balance with geostrophic winds

$$u_g = -\frac{1}{fa}\frac{\partial M}{\partial \varphi}, \tag{7}$$

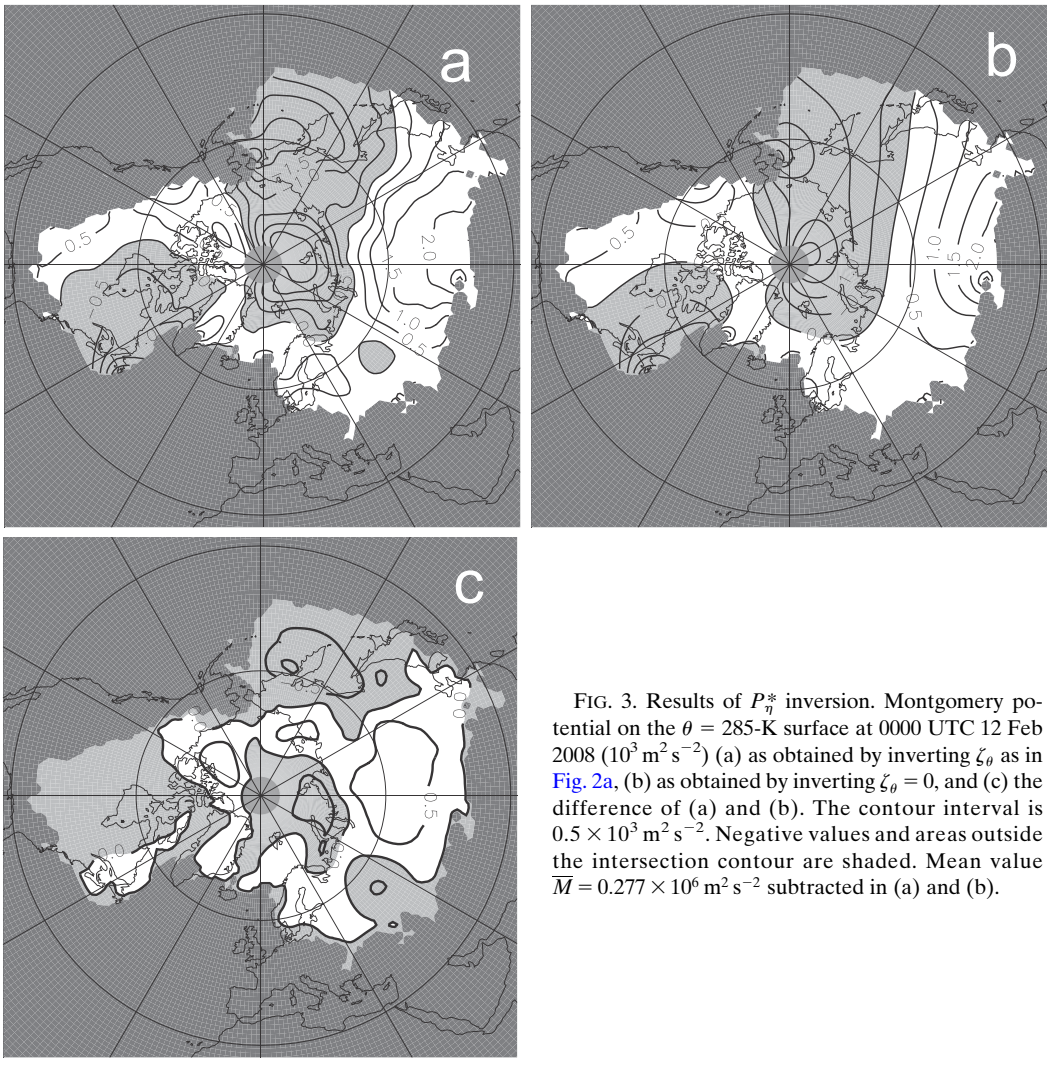

FIG. 3. Results of P_η^* inversion. Montgomery potential on the $\theta = 285$-K surface at 0000 UTC 12 Feb 2008 ($10^3\,\mathrm{m^2\,s^{-2}}$) (a) as obtained by inverting ζ_θ as in Fig. 2a, (b) as obtained by inverting $\zeta_\theta = 0$, and (c) the difference of (a) and (b). The contour interval is $0.5 \times 10^3\,\mathrm{m^2\,s^{-2}}$. Negative values and areas outside the intersection contour are shaded. Mean value $\overline{M} = 0.277 \times 10^6\,\mathrm{m^2\,s^{-2}}$ subtracted in (a) and (b).

$$v_g = \frac{1}{fa\cos\varphi}\frac{\partial M}{\partial \lambda}, \tag{8}$$

inversion of P_θ^* requires to solve

$$f^{-1}(a\cos\varphi)^{-2}\frac{\partial^2 M}{\partial \lambda^2} + a^{-2}(\cos\varphi)^{-1}\frac{\partial}{\partial \varphi}\left(f^{-1}\frac{\partial M}{\partial \varphi}\cos\varphi\right) = \zeta_\theta. \tag{9}$$

Observed values of M are prescribed where isentropic surfaces intersect the ground.

A circular domain of radius 450 km covering the North Pole is excluded from the inversion to avoid technical problems due to convergence of the meridians. Observed values of M are prescribed at this bounding circle. Relaxation with a convergence threshold of $\Delta M = 1\,\mathrm{m^2\,s^{-2}}$ yields the M patterns in Figs. 3 and 4, where the area-mean $\overline{M}$ has been subtracted. The inverted M field (Fig. 3a) satisfactorily approximates the observations in Fig. 2b. The inversion turns the complicated vorticity distribution in Fig. 2a into a relatively simple M pattern.

The role of the prescribed boundary values can be explored by inverting a vanishing relative vorticity $\zeta_\theta = 0$ (Fig. 3b) but keeping the same boundary values as in Fig. 3a. This inversion of boundary values is inspired by the standard practice in PVI to determine the impact of boundary values on distant flows (e.g., Davis and Emanuel 1991). This technique is partly motivated by the idea that potential temperature at the lower boundary can be interpreted as a PV anomaly that exerts an impact on the flow (Hoskins et al. 1985). Although this interpretation cannot be extended to our case, the boundary values of M indicate direction and intensity of the geostrophic flow across the boundary. Thus, inversions with $\zeta_\theta = 0$ tell us how these fluxes can be maintained by a flow in the interior without vorticity.

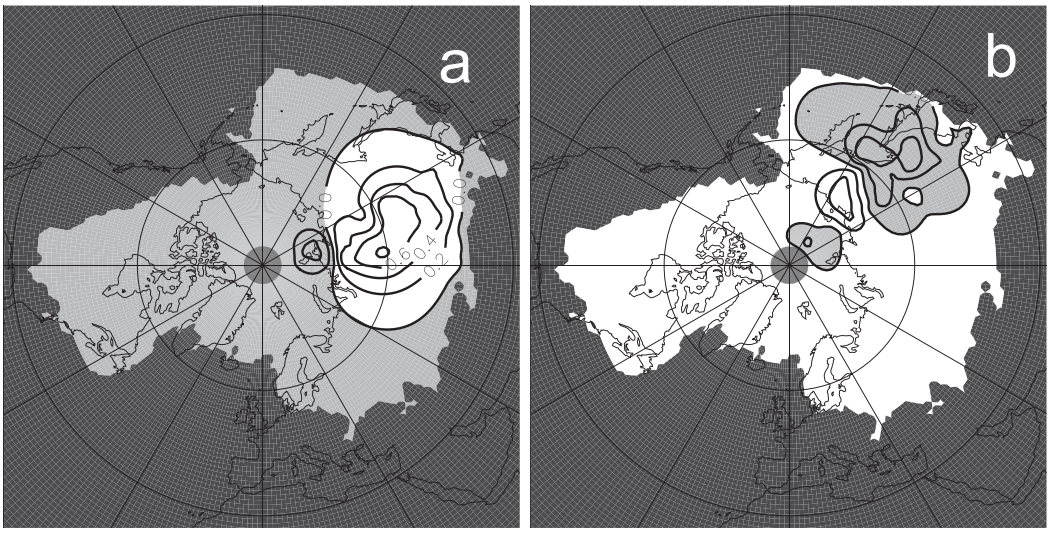

FIG. 4. Piecewise inversion of P_θ^* on $\theta = 285$-K surface at 0000 UTC 12 Feb 2008. Montgomery potential (10^2 m^2 s^{-2}) for $\zeta_\theta = 0$ except in the sector (a) $90° < \lambda < 120°$E and (b) $120° < \lambda < 150°$E. The contour interval is 0.2×10^2 m^2 s^{-2}. Negative values and areas outside the intersection contour are shaded.

A gross estimate of the response to boundary values can be based on *f*-plane solutions. In these cases, boundary perturbations of wavenumber k at a zonal boundary with meridional coordinate y decay proportional to $e^{-k|y-y_0|}$ away from the boundary at y_0. Thus, the smallest wavenumbers dominate the far field yielding a fairly smooth pattern away from the boundary.

The pattern in Fig. 3b is indeed quite smooth and the M values at the boundary extend far into the domain. Figures 3a and 3b are quite similar with positive values over Central Asia and a large depression extending from the Pacific across the North Pole as in Fig. 3a. In other words, the role of the boundary values in the inversion is at least as important as that of ζ_θ and amplitudes are generally small in the difference pattern in Fig. 3c. Note the reduced contour interval in Fig. 3c. We attribute this difference to the vorticity anomalies on the θ surfaces.

The height of the isentropic surface in Fig. 3a cannot be derived from the inverted M values on just one isentropic surface. We would have to solve (9) on a stack of θ surfaces so that the hydrostatic relation $\partial M/\partial\theta = c_p(p/p_0)^{R/c_p}$ can be used to determine the pressure, provided the surface temperature is known. With that, even Q_θ would be available and could be predicted using the available geostrophic winds.

Piecewise inversion has to select features of the vorticity field in Fig. 2a. Inversion is then performed with $M = 0$ at the boundaries. For example, the sector $90° < \lambda < 120°$E contains patches of negative relative vorticity, say, south of 70°N and a positive anomaly close to the North Pole. Figure 4a shows the Montgomery potential obtained with $M = 0$ at the boundaries, $\zeta_\theta = 0$ outside the domain 90°–120°E, and observed vorticity inside. The solution is centered in the longitude sector with a high in the south and a small low in the north, though the high extends into the adjacent sectors.

There are patches of strong positive vorticity in the sector 120°–150° (Fig. 2a), which correspond to the eastward-extending trough (Fig. 2b). The PPVDI results for this sector have also a low near the pole, which corresponds to a vorticity maximum there (see Fig. 4b).

Amplitudes in Fig. 4 are smaller but of the same order of magnitude as in Fig. 2b. That is to be expected, because the impact of the boundary values is missing in Fig. 4. Piecewise inversion could be performed for all latitude sectors, where superposition of all their results would give Fig. 3c. Comparison of Figs. 4a,b to Fig. 3c leads to the conclusion that the vorticity in one sector almost completely determines M in that sector in Fig. 3c.

b. *Inversion of P_p^**

Investigations of Q_p are relatively rare, though Haynes and McIntyre (1987) discussed fluxes of Q_p. Note that hydrostatic PVD and PV are the same for $\eta = p$ except for a factor ($P_p^* = -g\,Q_p$). Thus, PVI is the same as PVDI. The equation to be solved is (9), where we have to replace M by the geopotential ϕ and ζ_θ by ζ_p. The boundary conditions are the values of the geopotential at the boundary. We chose the 500-hPa surface, which rarely intersects the ground. The selected boundary contour is the same as before, which is an unusual choice for a pressure surface but was chosen to aid the comparison with the previous case. Such

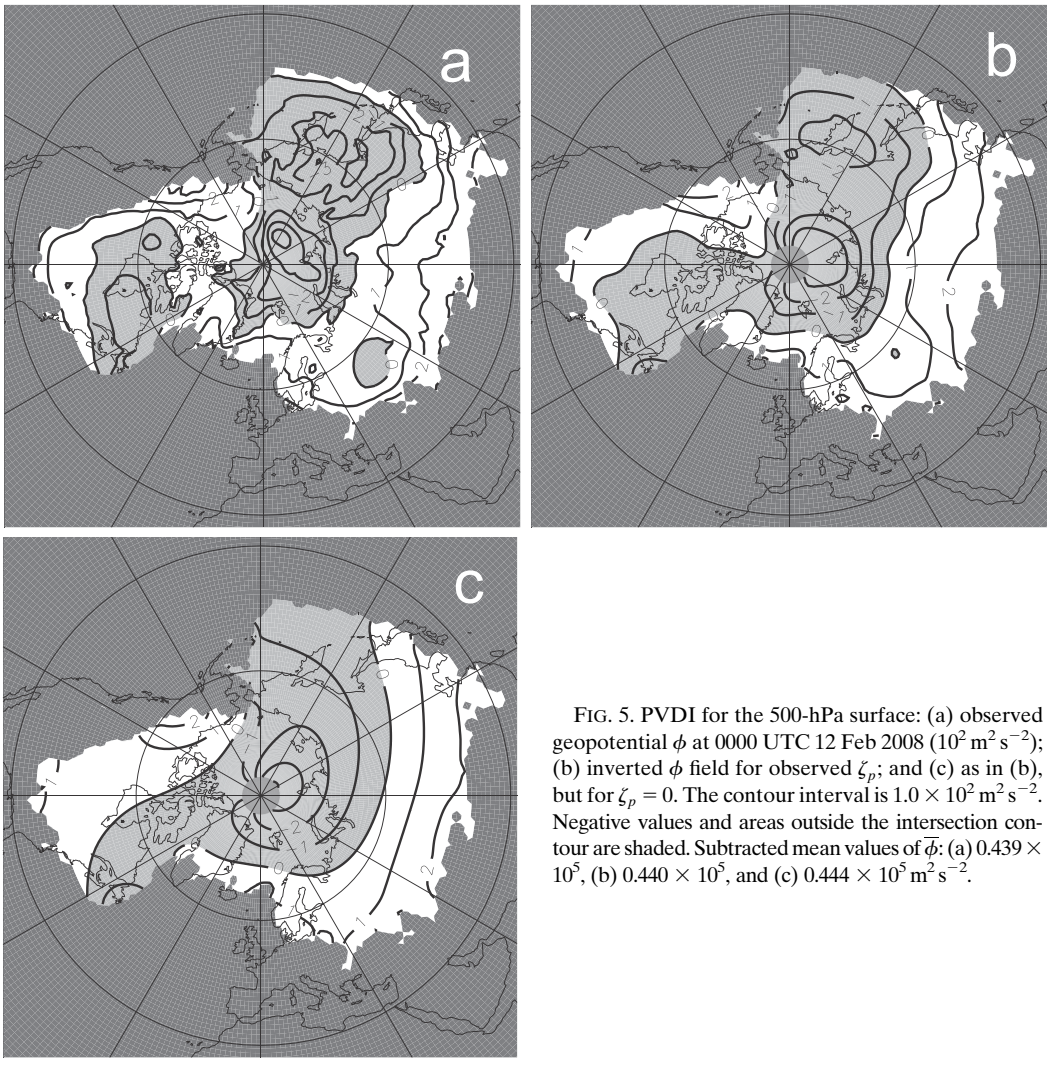

FIG. 5. PVDI for the 500-hPa surface: (a) observed geopotential ϕ at 0000 UTC 12 Feb 2008 ($10^2\,\mathrm{m^2\,s^{-2}}$); (b) inverted ϕ field for observed ζ_p; and (c) as in (b), but for $\zeta_p = 0$. The contour interval is $1.0 \times 10^2\,\mathrm{m^2\,s^{-2}}$. Negative values and areas outside the intersection contour are shaded. Subtracted mean values of $\overline{\phi}$: (a) 0.439×10^5, (b) 0.440×10^5, and (c) $0.444 \times 10^5\,\mathrm{m^2\,s^{-2}}$.

inversions have a long tradition and have been carried out routinely in the early one-layer models of numerical forecasting (Thompson 1961). It is nevertheless of interest to perform an inversion of P_p^* in parallel to P_θ^*.

The observed ϕ field in Fig. 5a is similar to the M pattern in Fig. 3a with an Asian ridge and lows at the North Pole, over North America, and over the Pacific. The inversion is again satisfactory (Fig. 5b) with a distinct Arctic low. The inversion for $\zeta_p = 0$ (Fig. 5c) yields a pattern that captures much of Fig. 5a and documents the importance of the lateral boundary values. As before, these boundary values of ϕ determine the geostrophic flows across the boundary. Areal mean values $\overline{\phi}$ have been subtracted for the respective fields. Note that the Arctic low has no closed height line in Fig. 5b, as is required for flows without vorticity. As the height of the p surfaces is given by the geopotential, PVDI in the isobaric case yields the complete information and we do not have to solve (9) for a stack of isobaric surfaces. Moreover, Q_p is readily available on this isobaric surface owing to the simple relationship with P_p^*.

3. Concluding remarks

This study has been stimulated by the well-known result that isentropic hydrostatic PVD P_θ^* reduces to a vorticity in isentropic coordinates. The variable η, as specified in the definition of Q_η, has been chosen as a vertical coordinate in extension of the isentropic case and the PVD P_η^* is considered instead of Q_η. The vorticity P_η^* turns out to be the absolute vertical vorticity component with respect to the basis $\mathbf{p}_i/|\mathbf{p}_i|$ of unit vectors aligned with the covariant basis. The nonhydrostatic terms of P_η^* can be important for strongly nonhydrostatic flows, such as in PV banners.

Three-dimensional PVI requires iterative methods to reconstruct the complete flow from the PV field in order to associate flow features with PV anomalies. The relatively simple structure of P_η^* in η coordinates, however, led us to consider the inversion of P_η^* on η surfaces, which reduces to a two-dimensional linear problem for hydrostatic flow. Such inversions have been carried out for $\eta = \theta$ and $\eta = p$. Geostrophic balance yielded satisfactory results in both cases. The role of the boundary values has been investigated by conducting inversions with $\zeta_\eta = 0$ in the domain. It turned out that a substantial part of the observed $M(\phi)$ field is related to the conditions at the boundaries, which represent the geostrophic wind across the boundaries and, thus, the dynamic interaction with the surrounding atmosphere.

We also conducted piecewise inversion to explore the role of isolated PV features. Examples of PPVDI have been presented, where we evaluated the geostrophic streamfunction associated with the vorticity in various longitude sectors and their extension into neighboring sectors.

Attribution appears to be straightforward in our case. The vorticity ζ_η on an η surface is a ''source'' for the flow on that surface, but boundary values are also important. On the other hand, inversion of Q_η would result in different attributions.

The simplicity of the hydrostatic P_η^* inversion in η coordinates is lost if we turn to nonhydrostatic flows. The contribution of w to P_η^* is difficult to evaluate, because the inversion becomes inherently nonlinear and three-dimensional [see Viúdez (2012) for nonhydrostatic inversions in a Boussinesq fluid].

Acknowledgments. We are grateful to two reviewers whose detailed comments helped to improve the paper. We would like to acknowledge the use of the ERA-Interim data produced and provided by ECMWF.

REFERENCES

Bracegirdle, T. J., and S. L. Gray, 2009: The dynamics of a polar low assessed using potential vorticity inversion. *Quart. J. Roy. Meteor. Soc.*, **135**, 880–893, doi:10.1002/qj.411.

Charney, J., 1955: The use of primitive equations of motion in numerical prediction. *Tellus*, **7**, 22–26, doi:10.1111/j.2153-3490.1955.tb01138.x.

Davis, C. A., 1992: Piecewise potential vorticity inversion. *J. Atmos. Sci.*, **49**, 1397–1411, doi:10.1175/1520-0469(1992)049<1397:PPVI>2.0.CO;2.

——, and K. A. Emanuel, 1991: Potential vorticity diagnostics of cyclogenesis. *Mon. Wea. Rev.*, **119**, 1929–1953, doi:10.1175/1520-0493(1991)119<1929:PVDOC>2.0.CO;2.

Dee, D. P., and Coauthors, 2011: The ERA-Interim reanalysis: Configuration and performance of the data assimilation system. *Quart. J. Roy. Meteor. Soc.*, **137**, 553–587, doi:10.1002/qj.828.

Egger, J., and K.-P. Hoinka, 2010: Potential temperature and potential vorticity inversion: Complementary approaches. *J. Atmos. Sci.*, **67**, 4001–4016, doi:10.1175/2010JAS3532.1.

Ertel, H., 1942: Ein neuer hydrodynamischer Wirbelsatz. *Meteor. Z.*, **59**, 277–281.

Haynes, P. H., and M. E. McIntyre, 1987: On the evolution of isentropic distributions of potential vorticity in the presence of diabatic heating and fictional or other forces. *J. Atmos. Sci.*, **44**, 828–841, doi:10.1175/1520-0469(1987)044<0828:OTEOVA>2.0.CO;2.

Hoskins, B. J., M. E. McIntyre, and A. W. Robertson, 1985: On the use and significance of isentropic potential vorticity maps. *Quart. J. Roy. Meteor. Soc.*, **111**, 877–946, doi:10.1002/qj.49711147002.

McIntyre, M. E., 2015: Potential vorticity. *Encyclopedia of Atmospheric Sciences*, 2nd ed. G. R. North, J. Pyle, and F. Zhang, Eds., Vol. 2, Elsevier, 375–383, doi:10.1016/B978-0-12-382225-3.00140-7.

Schär, C., M. Sprenger, D. Lüthi, Q. Jiany, R. Smith, and R. Benoit, 2003: Structure and dynamics of an alpine potential-vorticity banner. *Quart. J. Roy. Meteor. Soc.*, **129**, 825–855, doi:10.1256/qj.02.47.

Thompson, P., 1961: *Numerical Weather Analysis and Prediction.* MacMillan, 170 pp.

Thorpe, A., 1985: Diagnosis of balanced vortex structures using potential vorticity. *J. Atmos. Sci.*, **42**, 397–406, doi:10.1175/1520-0469(1985)042<0397:DOBVSU>2.0.CO;2.

Vallis, G., 2006: *Atmospheric and Oceanic Fluid Dynamics: Fundamentals and Large-Scale Circulation.* Cambridge University Press, 745 pp.

Viúdez, Á., 2001: The relation between Beltrami's material vorticity and Rossby Ertel's potential vorticity. *J. Atmos. Sci.*, **58**, 2509–2517, doi:10.1175/1520-0469(2001)058<2509:TRBBMV>2.0.CO;2.

——, 2012: Potential vorticity and inertia–gravity waves. *Geophys. Astrophys. Fluid Dyn.*, **106**, 67–88, doi:10.1080/03091929.2010.537265.

Zdunkowski, W., and A. Bott, 2003: *Dynamics of the Atmosphere: A Course in Theoretical Meteorology.* Cambridge University Press, 719 pp.